Numerical simulation of regional circulation in the Monterey Bay region

By Y. H. Tseng, D. E. Dietrich †, AND J. H. Ferziger

1. Motivation and objectives

Monterey Bay is located 100 km south of San Francisco and is one of several large bays on the West Coast of the United States. This area is important due to the abundance of marine life. The regional circulation in the Monterey Bay area is tightly coupled to the California Current System (CCS) and highly correlated to the coastal upwelling. In the offshore region, flow is dominated by a broad, weak, equatorward flowing current, the California Current (CC). The CC extends offshore to a distance of $900 - 1000$ km and flows year-round. Within about 100 km of the coast, two narrow poleward flowing boundary currents have been found, the Inshore Countercurrent (IC) and the California Undercurrent (CU). The IC is a weak current that varies seasonally, appearing in fall and winter, and transports shallow, upper layer water. The CU is a narrow ($10 - 50$ km) relatively weak subsurface flow and transports warm, saline equatorial water. The CU is strongest at around $100 - 300$ m depth and has a mean speed of approximately 15 cm/s (Pierce *et al.* 2000) at all latitudes on the West Coast throughout the year.

While many experimental studies have examined the flow in the vicinity of Monterey Bay, there are only a few numerical studies focusing on the regional circulation. These previous modeling studies have mostly used simplified dynamics, domains, and forcing, with coarse spatial resolution or/and short integration times. However, there are some significant interannual variations, including large scale effects relating to El Nino/Southern Oscillation dynamics and smaller scale noise due to fronts and eddies. The regional circulation in this region is very complex and difficult to model correctly.

The objective of this study is to produce a high-resolution numerical model of Monterey Bay area in which the dynamics are determined by the complex geometry of the coastline, steep bathymetry, and the influence of the water masses that constitute the CCS. Our goal is to simulate the regional-scale ocean response with realistic dynamics (annual cycle), forcing, and domain. In particular, we focus on non-hydrostatic effects (by comparing the results of hydrostatic and non-hydrostatic models) and the role of complex geometry, i.e. the bay and submarine canyon, on the nearshore circulation. To the best of our knowledge, the current study is the first to simulate the regional circulation in the vicinity of Monterey Bay using a non-hydrostatic model. Section 2 introduces the high resolution Monterey Bay area regional model (MBARM). Section 3 provides the results and verification with mooring and satellite data. Section 4 compares the results of hydrostatic and non-hydrostatic models. Finally, conclusions and future work are drawn in section 5.

† AcuSea Inc., Albuquerque, New Mexico

2. Monterey Bay area regional model (MBARM)

2.1. *Numerical methods*

In order to study the regional circulation in the vicinity of Monterey Bay while avoiding numerical errors introduced by the σ-coordinate and non-hydrostatic effects, we used the non-hydrostatic, z-level, mixed Arakawa A and C grid, fourth-order accurate Dietrich/Center for Air-Sea Technology (DieCAST) ocean model, which provides high computational accuracy and low numerical dissipation and dispersion. The numerical procedures are detailed in Dietrich & Lin (2002) and Tseng (2003).

The Coriolis terms are evaluated on the 'a' grid and thus have no spatial interpolation error, which is a significant advantage for a dominant term (Dietrich 1997). Fourth-order central differencing is used in the control volume approximation to compute all advection and horizontal pressure gradient terms, except adjacent to boundaries where second-order accuracy is used. All control volumes are collocated (e.g. momentum, energy, salinity and the incompressibility approximation to mass conservation) and are all enforced on the same set of control volumes. The model uses a rigid-lid approximation. At the regional ocean scale, the 'slow modes' (low frequency, long time scale motions) dominate the ocean circulation. Use of a rigid lid excludes the 'fast mode' associated with barotropic free surface waves. The rigid-lid approximation does not affect internal gravity wave speeds. Thus, it does not affect geostrophic adjustment of the baroclinic mode that dominates the general circulation. The rigid-lid approximation also simplifies the treatment of open boundaries because it greatly reduces the range of frequencies that must be addressed.

2.2. *Model descriptions*

The Monterey Bay area regional model (MBARM) is one-way coupled to a larger scale California current system DieCAST model and uses the immersed boundary method to represent the coastal geometry and bathymetry (Tseng & Ferziger 2003) in the local model. The domain of MBARM extends from 36.1° to $37.4^\circ N$ and from the California coast out to $122.9^\circ W$ (Figure 1); the horizontal grid size is uniformly $1/72^\circ$ ($\approx 1.5\ km$) for the medium grid, and $1/108^\circ$ ($\approx 1\ km$) for the fine grid. The vertical grid has 28 levels. The surface buoyancy flux is computed by nudging both the temperature and the salinity toward Levitus' monthly climatology (Levitus 1982). This is equivalent to adding heat and/or freshwater to the top layer. This salinity condition, although widely used, has little physical basis and does not conserve salt material exactly (Dietrich *et al.* 2003), but it has little effect in the region modeled because the salinity field is strongly constrained by the open boundary inflows; freshwater sources from rivers and precipitation, and sinks from evaporation have only minor effect in this region. The wind stress is from Hellerman and Rosenstein's monthly climatology (Hellerman & Rosenstein 1983). The southeastward winds intensify during spring and summer and weaken during fall and winter.

Bathymetry is unfiltered USGS 250 m resolution topography. The bottom topography and the coastal geometry are adequately represented by the immersed boundary module (Tseng & Ferziger 2003). The sea floor is insulated and partial-slip as parameterized by a nonlinear bottom drag coefficient of 0.002. Significant momentum exchange with the California Current System occurs through the open boundary.

The model is one-way coupled from a larger scale CCS model (Haney *et al.* 2001) which has resolution $1/12^\circ$. The MBARM is initialized by interpolation of the coarse CCS model results after two years of simulation. All open boundary conditions are based on boundary fluxes. A pure upwind advective scheme is used at the three lateral open

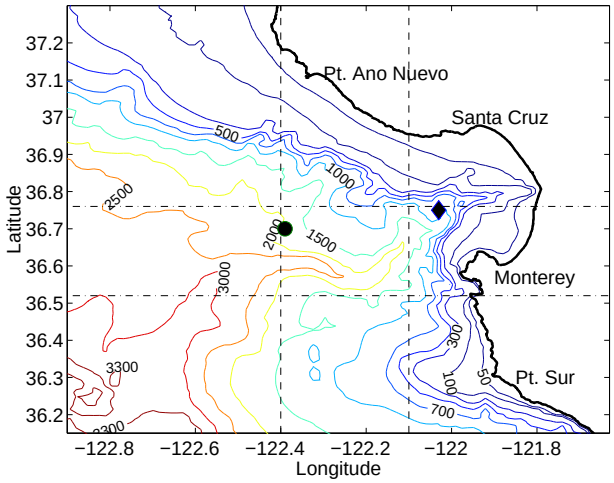

FIGURE 1. The model domain of Monterey Bay area and bathymetry. Locations of moorings M1, M2 are marked by a circle and a diamond, respectively. '−.': lines at latitude $36.52°N$ and $36.76°N$, '−−': lines at longitude $122.4W$ and $121.1°W$. The horizontal uniform grid is shown by the dotted lines (Every sixth grid is shown).

boundaries (north, south, and west) for all variables:

$$\frac{\partial \phi}{\partial t} + U_n \frac{\partial \phi}{\partial n} = 0 \tag{2.1}$$

where

$$\frac{\partial \phi}{\partial n} = \begin{cases} (\phi - \phi_o)/\Delta x_n & U_n \geq 0 \\ (\phi_i - \phi)/\Delta x_n & U_n < 0 \end{cases} \tag{2.2}$$

and U_n is the normal velocity on the open boundary. ϕ represents any of the three velocity components, temperature or salinity at the boundary. ϕ_o is the variable on the open boundary obtained from the CCS model and ϕ_i is the variable at one grid point inside the open boundary, Δx_n is the grid spacing in the direction normal to the boundary. Thus, large scale data are advected inward at an inflow boundary and the interior data is advected outward at an outflow boundary.

It has been argued that the primitive equations are ill-posed when an inappropriate open boundary condition is used. If the proper number of boundary conditions is not specified, the solution of the primitive equations will lead to the exponential growth of energy and numerical instability (Oliger & Sundstrom 1978). According to Oliger & Sundstrom (1978) and Mahadevan *et al.* (1996), the numerical problem is well-posed if the velocity vector, salinity, and temperature are specified at the inflow boundary condition and the normal velocity is specified at the outflow boundary. The above open boundary treatment satisfies these requirements and is well-posed. Palma & Matano (2000) investigated the performance of combinations of OBCs using POM. They found that the best overall performance of OBCs was a flow relaxation scheme for barotropic modes, a radiation condition for baroclinic modes, and combined advection and relaxation for the scalar field. In fact, the current scheme corresponds to a simplified version of the scheme suggested by Palma & Matano (2000).

3. Results

3.1. *General description*

Using Levitus' surface climatological forcing (temperature and salinity), the simulation reproduces many important features of the observed annual cycle of the CCS including the strengthening of the equatorward jet in spring and the weakening of the jet in autumn and winter. Coastal eddies occur primarily near some major headlands, especially Point Ano Nuevo, Pacific Grove and Point Sur. To examine the general circulation in the vicinity of Monterey Bay, we focus on the annual mean flow and seasonal variability.

3.1.1. *Annual mean flow*

The mean velocity fields for a simulation year at various depths (10.1, 50, 100, 300, 400, 700 m) are shown in Figure 2. As mentioned before, the major features in the Monterey Bay area are the shallow, equatorward, broad California Current and two narrow poleward boundary currents (California Undercurrent and Inshore Current) along the coast. These flows are seen in Figure 2. The surface flow is affected by surface wind forcing. Vertical shear layers appear at moderate depth ($50-200\ m$). The mean velocity pattern clearly delineates the extent of poleward flow associated with the inshore currents.

Collins *et al.* (2000) estimated the upper 1000 m depth-averaged mean velocity based on 19 cruises conducted from April 1988 to April 1991. They reported a west-northwestward ($290°T-310°T$) flow with a mean speed of $3.7-5.3\ cm/s$ at four inshore stations C1-C4 (at latitude $36.3°N$, $33-65\ km$ away from the shore). We estimate the one-year depth-averaged annual mean flow along the line connecting the four inshore stations C1-C4 (Collins *et al.* 2000). The mean magnitude is $4.7\ cm/s$ with direction $301°T$. The annual mean flow in the current study is in good agreement with observation. The result shows that the current one-way coupling at lateral boundary and the surface forcing are appropriate. More detailed comparison with observation is provided in the following section.

3.1.2. *Seasonal variability*

Summer and winter mean velocity fields at several depths (10.1, 100, 300, 700 m) are shown in Figures 3 and 4 for a simulation year. The along-shore component of the wind stress has been shown to be a key ingredient for generating realistic vertical and horizontal structures and the surface equatorward and subsurface poleward currents. These currents are baroclinically and barotropically unstable, resulting in the generation of meanders, filaments and eddies.

In summer, defined as May to July (Figure 3), the equatorward flow strengthens and dominates the flow from a depth of 100 m to the surface. This equatorward flow is forced by upwelling-favorable winds. A weak cyclonic eddy is observed within Monterey Bay, and is associated with the equatorward flow past a coastal bay. There is also a large-scale, anti-cyclonic eddy around 50 km from the coast that extends down to depth 100 m where the eddy is stretched significantly by the coastal bathymetry. The subsurface northward flow exists below depth 300 m during spring which is consistent with the year round northward flow associated with the CU. The transition from CC to CU occurs around depth $200-500\ m$ and the strongest CU occurs at depth 300 m, which is consistent with previous observations. These flows are tightly coupled with the large scale California current system model through open boundary.

The southward flow in the upper ocean strengthens and tends to move offshore, forming the filaments observed in the satellite images. Point Sur is the location where the

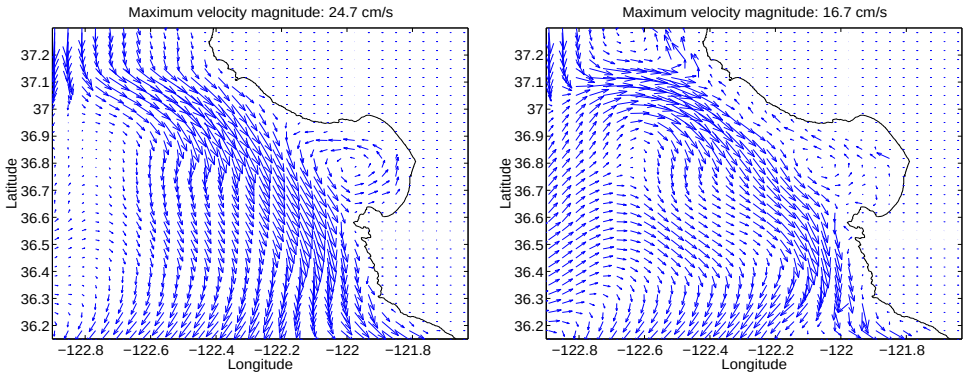

(a) (b)

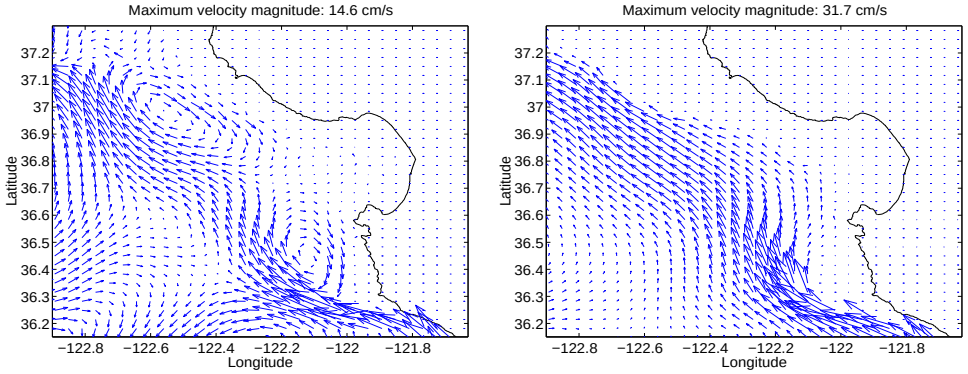

(c) (d)

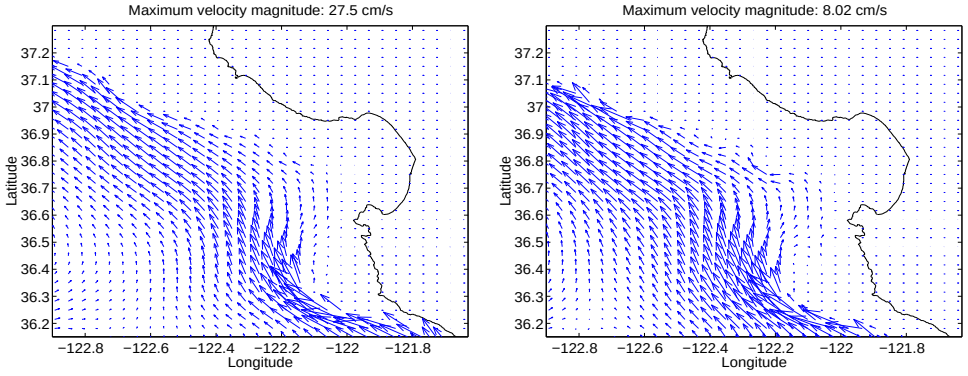

(e) (f)

FIGURE 2. The annual mean velocity field at various depths for a year. At depth (a) 10.1 m, (b) 50 m, (c) 100 m, (d) 300 m, (e) 400 m,(f) 700 m.

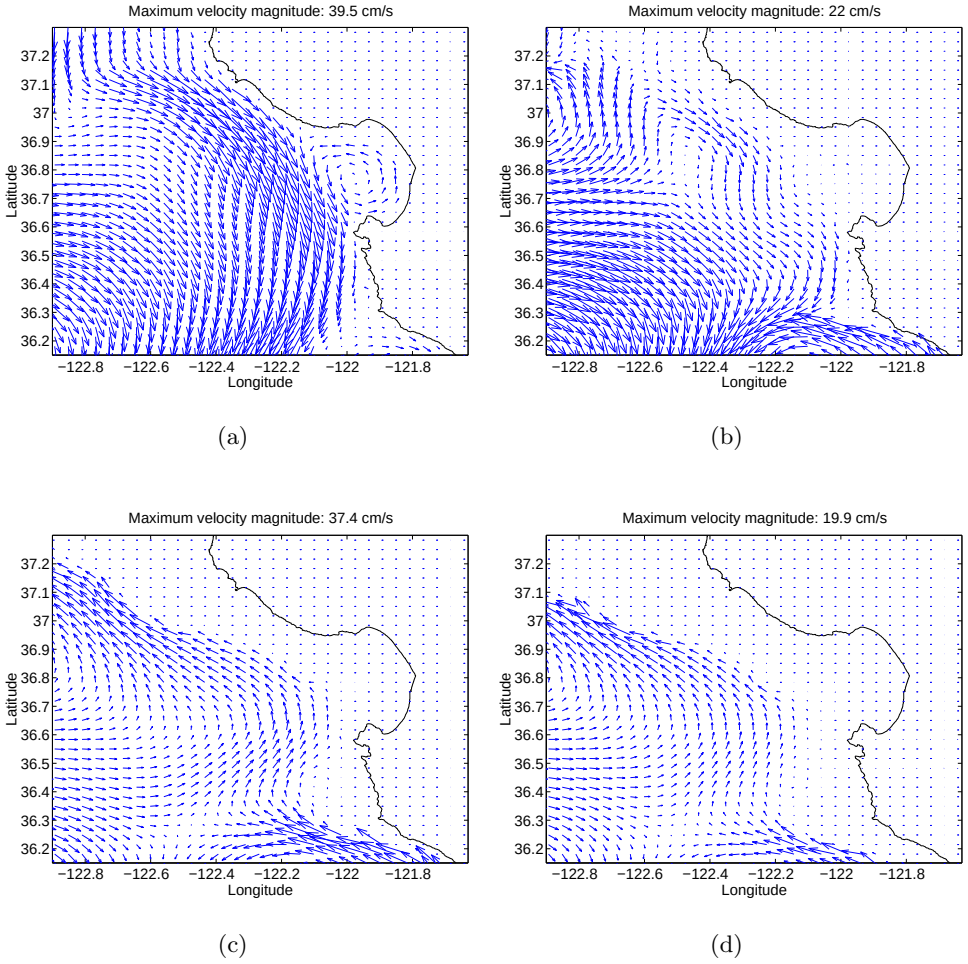

FIGURE 3. The mean velocity field at various depths during summer. At depth (a) 10.1 m, (b) 100 m, (c) 300 m, (d) 700 m.

offshore flow is most significant and satellite images also show that filaments occur there frequently. The current simulation shows this to be an effect of local topography on the enhancement of flow toward steep bathymetry and the steering effect of the Pacific Grove headland. The same conclusion was suggested by observations (Ramp *et al.* 1997). We still see the CU at depth, and the undercurrent follows the contours of coastal bathymetry closely.

Autumn is the season in which the dominant flow changes from equatorward to poleward in the upper ocean. By October upwelling favorable circulation occurs much less frequently, and near-surface flow along the central coast is under the influence of the northward flowing Davidson Current, which generally reaches its maximum speed at the surface in December. Figure 4 shows the mean flow in wintertime (November to January) at several depths. The velocity fields at all levels show very similar spatial structure. The CCS is dominated by the poleward flow. A narrow equatorward flow can still be observed

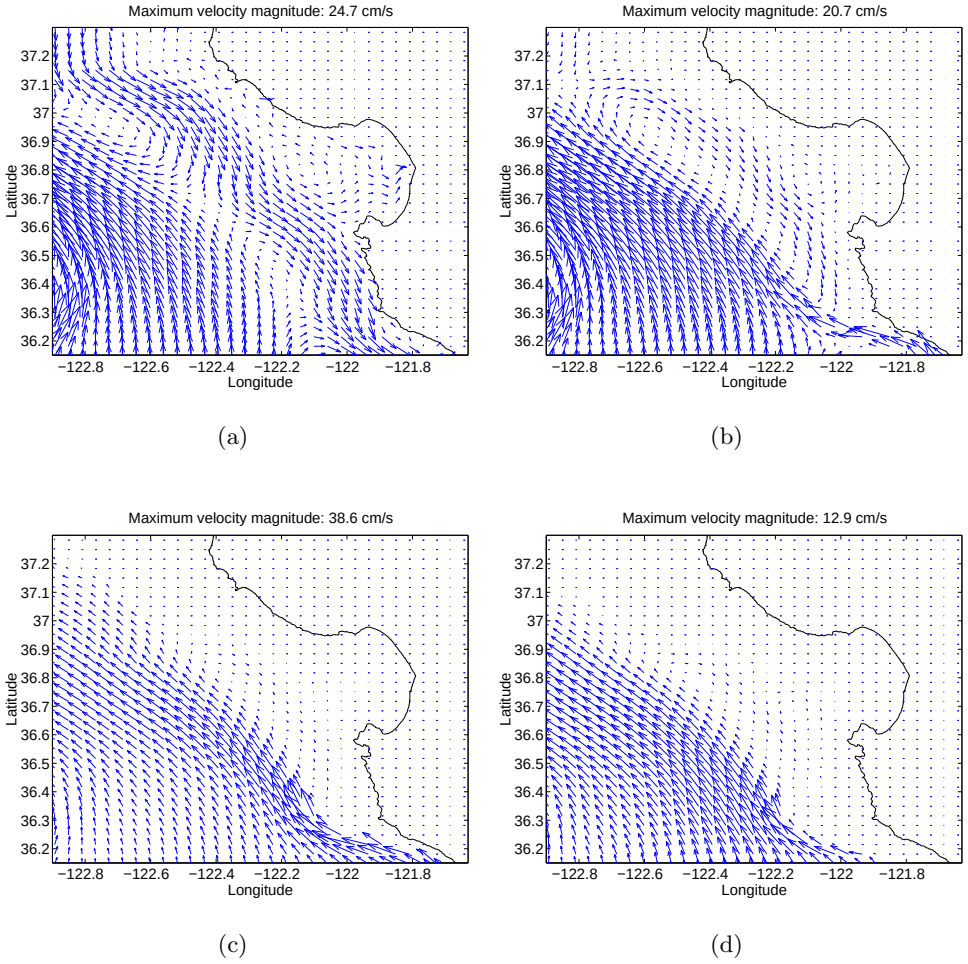

FIGURE 4. The mean velocity field at various depths during winter. At depth (a) 10.1 m, (b) 100 m, (c) 300 m, (d) 700 m.

in the shallow region. The poleward currents off Point Sur usually flow toward the northwest (along-shore), while the summer equatorward currents flow toward the southwest rather than southeastward along the large-scale bathymetry. This feature of the flow is reproduced by the simulation and can likely be attributed to the local topography, which tends to steer currents from the north offshore (Ramp *et al.* 1997).

3.2. *Comparison with mooring data*

We compare the model temperatures with those measured by Sea-Bird MicroCAT CTDs mounted on MBARI's M1 (122.03°W, 36.75°N) and M2 (122.39°W, 36.70°N) surface moorings (for location, see Figure 1). Since the model is forced by the average climatology at the sea surface, we do not expect the model to match the observations exactly.

The observed time series of temperatures at the M1 and M2 mooring stations display an annual cycle with cold temperatures during upwelling seasons and warmer temperatures during the rest of the year. The seasonal variation is more significant near the surface than

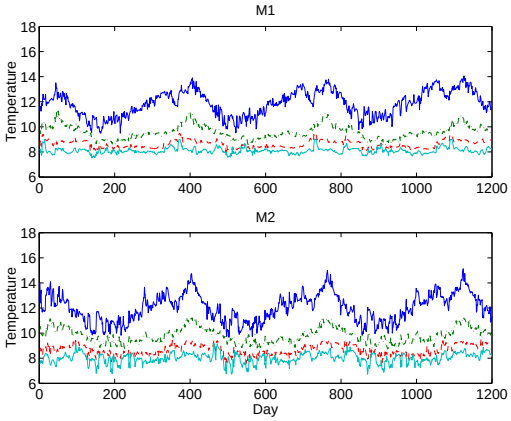

FIGURE 5. Model time series of temperature at stations M1 (top) and M2 (bottom) for three simulation years. The model repeats smoothly after 40 days, thus showing that the annual cycle is accurately responded. The depths from top to bottom are 10 m, 100 m, 200 m and 300 m.

at depth. The model results are shown in Figure 5 for the M1 and M2 mooring locations, respectively. The results repeat annually, showing that the model has been run long enough that the results are independent of the initial state. The model results reproduce many of the observed trends. These include the annual variation in temperature, cooling of surface and subsurface temperatures during spring upwelling, warming water masses during summer and early autumn, and slight cooling during late autumn. The near surface temperature (10 m) at M2 varies between $10-15^{\circ}$ which is in the same range as the observations. The temperature at M1 is $1-2^{\circ}$ lower than that at M2, which is again consistent with the measurements. At depth 300 m, the temperature varies from $7-9^{\circ}$ at both the M1 and M2 stations, consistent with the observational data. The most important result of the simulation is the fact that, as in the observation, the annual cycle is evident and well reproduced in the simulation.

3.3. *Comparison with other observation results*

During periods of upwelling-favorable winds (spring and summer), there is a band of cold water which flows equatorward across the mouth of Monterey Bay with typical near-surface speeds of $20-30 cm/s$. Figures 6(a)-(b) show the surface temperature for day 109 and day 113 and contain a typical spring upwelling event. The upwelling centers are found north and south of Monterey Bay near Points Ano Nuevo and Sur (Figure 6(b)). Point Ano Nuevo has been identified to be the source of cold, salty near-surface water frequently seen in the bay (Rosenfeld *et al.* 1994). The upwelled (cold) water is advected southward across the bay and then breaks into two streams: one water mass moves offshore and the other equatorward. A warm anticyclonic feature is often found off the mouth of Monterey Bay, or just south of it (Ramp *et al.* 1997). This feature was also seen in advanced very high resolution radiometer (AVHRR) imagery. The simulation produces patterns very similar to those observed in the satellite images. A warm anticyclone is also apparent in the simulation. Meanders of the California current with anticyclonic circulation have often been reported (Breaker & Broenkow 1994; Ramp *et al.* 1997).

Within the bay, a cyclonic circulation is often observed (Breaker & Broenkow 1994). This circulation is caused mainly by the coastal geometry. The cyclonic circulation within Monterey Bay is consistent with the observed circulation.

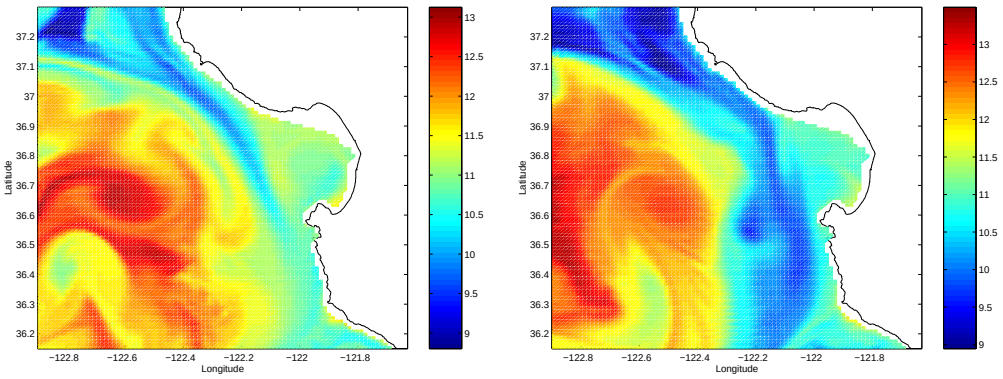

(a) Day 109 (b) Day 113

FIGURE 6. The surface temperature field for day 109 and day 113.

4. Hydrostatic versus Non-Hydrostatic modeling

The growth of meanders and filaments of upwelled water has been demonstrated in many previous studies using hydrostatic models. However, it is still not clear how the non-hydrostatic mode affects the circulation in a coastal region with complex bathymetry and upwelling. Casulli & Stelling (1998) assessed the effects of the hydrostatic approximation in various applications and found that the hydrostatic model is not accurate in some cases. The hydrostatic approximation breaks down when the vertical acceleration is significant compared to the buoyancy force.

The vertical momentum and the non-hydrostatic pressure component cannot be neglected when the bottom topography changes abruptly on scales small compared to the local Rossby radius of deformation (e.g. near continental shelf edges and in deep canyons). Chao & Shaw (2002) studied coastal upwelling meanders and filaments using a non-hydrostatic model. Their idealized model does not include complex bathymetry, coastal irregularity or unsteady wind forcing. Their results show that the growth rates of meanders and filaments are enhanced by non-hydrostatic effects. Here we explore the impact of the hydrostatic approximation by comparing results from hydrostatic and non-hydrostatic versions of the DieCAST model applied to Monterey Bay.

It is noteworthy that hydrostatically modeled systems actually have more total energy than the corresponding non-hydrostatic systems. Specifically, the potential energy decrease due to sinking dense fluid and rising warm fluid goes entirely into horizontal kinetic energy according to the hydrostatic equations. Vertical acceleration senses no inertia, generally leading to larger vertical acceleration than would occur when inertia terms are included in the vertical momentum equation. The hydrostatic approximation is well posed and robust in spite of its lack of energy conservation; the horizontal kinetic energy is limited by the potential energy release and the vertical kinetic energy is limited, in turn, by its relation to horizontal velocity through the incompressibility equation.

The vertical velocity differences between the hydrostatic and non-hydrostatic models at various depths are shown in Figure 7. They are large along the canyon wall at all depths. These results show that rapid changes in slope cause vertical accelerations which violate the hydrostatic approximation. Vertical acceleration associated with the bores produced

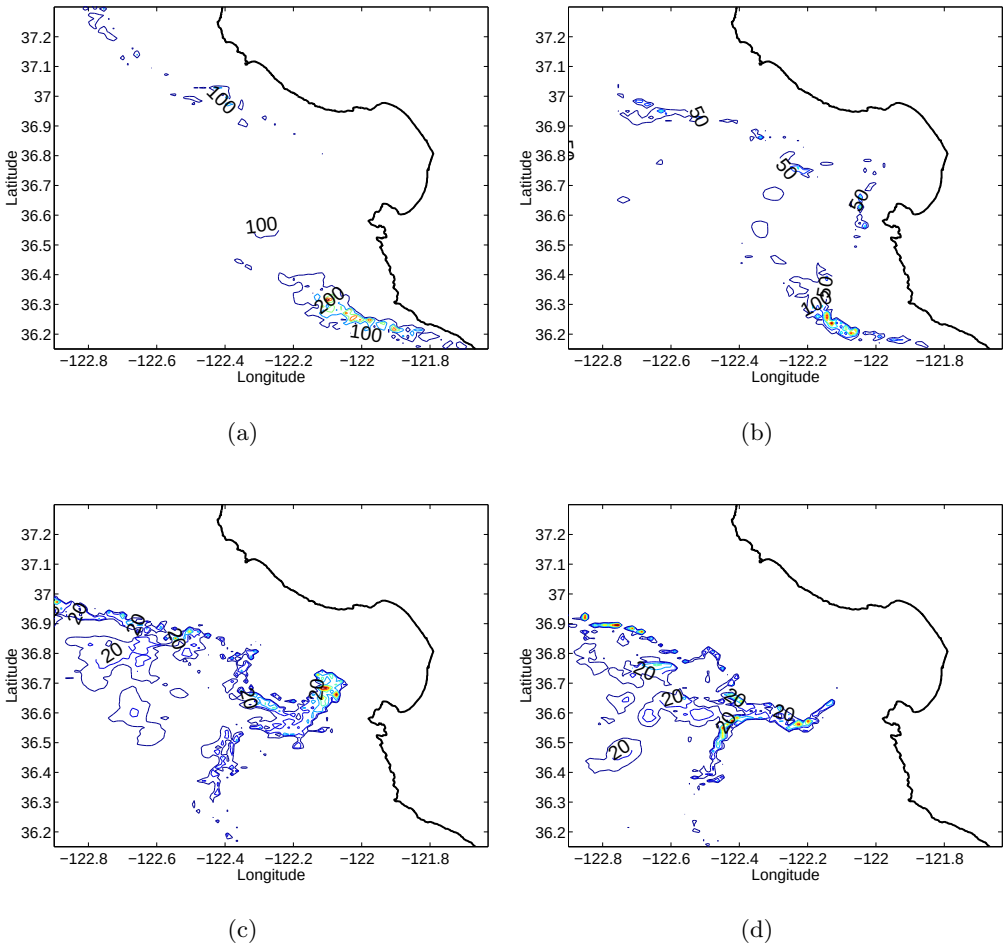

FIGURE 7. The contour of vertical velocity difference ($m/week$) between the hydrostatic and non-hydrostatic models at various depths. (a) 100 m, (b) 700 m, (c) 1500 m, (d) 2000 m, The difference is based on monthly averaged vertical velocity during June (day 150-180).

by internal wave reflection at topography is also poorly represented by the hydrostatic model (Legg & Adcroft 2003). In realistic topography, alongslope tides produce internal hydraulic jumps and solitary wave packets as they flow over corrugations. This is not well represented by hydrostatic models.

5. Conclusion and future work

The high resolution, non-hydrostatic MBARM was used to investigate the regional ocean circulation in the Monterey Bay area. The model reproduces several known features of the general circulation in the vicinity of Monterey Bay. The Monterey Bay area circulation is highly correlated to the CCS so the surface flow pattern in spring/summer is different from that in autumn/winter. Within the bay a cyclonic circulation is often

observed. This feature is a result of coastal geometry. A warm anticyclone is often seen near the mouth of Monterey Bay. In particularly, non-hydrostatic effects play an important role in determining the non-linear dynamics of the nearshore circulation. The non-linear non-hydrostatic dynamics are enhanced by the complex coastal geometry and cannot generally be ignored in regions of steep bathymetry or where the Rossby radius of deformation is small; sometimes it is even negative, leading to strongly nonhydrostatic convection.

The current MBARM uses one-way coupling to allow information from the CCS to enter the coastal region. In order to examine their dynamical interactions, full two-way coupling is needed in the future. Two-way nesting will generate much smoother results and remove artificial fronts when the boundary flow switches between outflow and inflow. To better understand the dynamics of the coastal region, which is strongly affected by coastal perturbations and bathymetry, non-hydrostatic effects should be further investigated using non-hydrostatic coastal model with simplified coastal geometry, e.g. an idealized bay and an idealized submarine canyon. The current simulation results identify some important non-hydrostatic effects. However, realistic topography and forcing complicate the analysis and understanding of the physical process. Detailed analysis is required to quantify non-hydrostatic effects on the overall circulation.

REFERENCES

Breaker, L. C. & Broenkow, W. W. 1994 The circulation of Monterey Bay and related processes. *Oceanogr. and Marine Bio.* **32**, 1-64.

Casulli, V. & Stelling, G. S. 1998 Numerical simulation of 3D quasi-hydrostatic, free-surface flow. *J. Hydrau. Eng.* **124**, 678-686.

Chao, S. Y. & Shaw P. T. 2002 Nonhydrostatic aspects of coastal upwelling meanders and filaments off eastern ocean boundaries. *Tellus* **54(A)**, 63-75.

Collins, C. A., Garfield, N., Rago, T. A., Rischmiller, F. W. & Carter, E. 2000 Mean structure of the inshore countercurrent and California undercurrent off Point Sur, California. *Deep-Sea Res. II* **47**, 765-782.

Dietrich, D. E. 1997 Application of a modified "a" grid ocean model having reduced numerical dispersion to the gulf of Mexico circulation. *Dyn. Atmos. Oceans* **27**, 201-217.

Dietrich, D. E. & Lin, C. A. 2002 Effects of hydrostatic approximation and resolution on the simulation of convective adjustment. *Tellus* **54(A)**, 34-43.

Dietrich, D. E., Haney, R. L., Fernandez, V., Posey, S. & Tintore, J. 2003 Model-determined surface heating and freshwater sources using a precise, non-damping nudging approach. *J. Mar. Systems (accepted).*

Haney, R. L., Hale, R. A. & Dietrich, D. E. 2001 Offshore propagation of eddy kinetic energy in the California Current. *J. Geophys. Res.* **106**, 11709-11717.

Hellerman, S. & Rosenstein, M. 1983 Normal monthly wind stress over the world ocean with error estimates. *J. Phys. Oceanogr.* **13**, 1093-1104.

Legg, S. & Adcroft, A. 2003 Internal wave breaking at concave and convex continental slopes. *J. Phys. Oceanogr.* **33**, 2224-2246.

Levitus, S. 1982 Climatological atlas of the world oceans. *NOAA Prof. Pap.* U.S. Govt. Print Off., 173.

Mahadevan, A. and Oliger, J. & Street, R. L. 1996 A nonhydrostatic mesoscale ocean model. Part I: Well-posedness and scaling. *J. Phys. Oceanogr.* **26**, 1868-1880.

Oliger, J. & Sundstrom, A. 1978 Theoretical and practical aspects of some initial boundary value problems in fluid dynamics. *SIAM J. Appl. Math.* **35**, 419-446.

Palma, E. D. and Matano, R. P. 2000 On the implementation of open boundary condition for a general circulation model: The three-dimensional case *J. Geophys. Res.* **105**, 8605-8627.

Pierce, S.D. , Smith, R. L., Kosro, P. M., Barth, J. A. & Wilson, C. D. 2000 Continuity of the poleward undercurrent along the eastern boundary of the mid-latitude Pacific. *Deep-Sea Res. II* **47**, 811-829.

Ramp, S. R., Rosenfeld, L. K., Tisch, T. D. & Hicks, M. R. 1997 Moored observations of the current and temperature structure over the continental slop off central California, 1, A basic description of the variability. *J. Geophys. Res.* **102**, 22877-22902.

Rosenfeld, L. K., Schwing, F. B., Garfield, N. & Tracy, D. E. 1994 Bifurcated flow from an upwelling center: A cold water source for Monterey Bay. *Cont. Shelf Res.* **14**, 931-964.

Tseng, Y. H. & Ferziger, J. H. 2003 A ghost-cell immersed boundary method for flow in complex geometry. *J. Compu. Phys. (in press).*

Tseng, Y. H. 2003 *On the development of a ghost-cell immersed boundary method and its application to large eddy simulation and geophysical fluid dynamics.* Ph. D. Dissertation, Stanford University.